Spectrochimica Acta Part A: Molecular and Biomolecular Spectroscopy 188 (2018) 372–381

Contents lists available at ScienceDirect

Spectrochimica Acta Part A: Molecular and Biomolecular Spectroscopy

journal homepage: www.elsevier.com/locate/saa

Optoelectronic performance comparison of new thiophene linked benzimidazole conjugates with diverse substitution patterns

Gözde Murat Saltan [a], Haluk Dinçalp [a,*], Eser Kırmacı [a], Merve Kıran [b], Ceylan Zafer [b]

[a] Department of Chemistry, Faculty of Arts and Science, Manisa Celal Bayar University, Yunus Emre, 45140 Manisa, Turkey
[b] Solar Energy Institute, Ege University, Bornova, 35100 Izmir, Turkey

ARTICLE INFO

Article history:
Received 19 December 2016
Received in revised form 24 June 2017
Accepted 11 July 2017
Available online 13 July 2017

Keywords:
Optoelectronic materials
Intramolecular charge transfer
Dual luminescence
Thin films
Photovoltaic

ABSTRACT

In an approach to develop efficient organic optoelectronic devices to be used in light-driven systems, a series of three thiophene linked benzimidazole conjugates were synthesized and characterized. The combination of two thiophene rings to a benzimidazole core decorated with different functional groups (such as —OCH_3, —$N(CH_3)_2$, —CF_3) resulted in donor-acceptor type molecular scaffold. The effect of the electronic behavior of the substituents on the optical, electrochemical, morphological and electron/hole transporting properties of the dyes were systematically investigated. **DTBI2** dye exhibited distinct absorption properties among the other studied dyes because *N*,*N*-dimethylamino group initiated intramolecular charge transfer (ICT) process in the studied solvents. In solid state, the dyes exhibit peaks extending up to 600 nm. Depending on the solvent polarities, dyes show significant wavelength changes on their fluorescence emission spectra in the excited states. Morphological parameters of the thin films spin-coated from $CHCl_3$ solution were investigated by using AFM instrument; furthermore photovoltaic responses are reported, even though photovoltaic performances of the fabricated solar cells with different configurations are quite low.

1. Introduction

Benzimidazole, naturally found in the core structure of the vitamin B_{12} and coenzyme B_{12}, is a type of ligand which is generally used in the complex formation. Their hydroxylated derivatives are ligands suitable for chelating with different metal ions due to their strong π–conjugation properties [1–4]. Benzimidazoles are known as suitable groups for optoelectronic applications because of their high fluorescence quantum yields [5] and wide ranges of Stokes shift values. They give a wide variety of broad UV–vis absorption bands around 450 nm and different line shapes depending on the substituents attached onto the benzimidazole ring. Their aromatic core structures have been attained since it can be variously functionalized on their C-2 placement [6,7].

Novel class of organic semiconductors is in progress for the development of inexpensive and high performance optoelectronic materials. Organic photovoltaics (OPVs) have been attracting substantial interest due to their important rewards of low-priced, lightweight and favorable solution processability as well as their potential application in ink-jet printing and roll-to-roll technique for flexible large-area devices. Both new donor and acceptor materials for OPVs with effective extinction coefficients, high stabilities and good film morphologies are needed to catch up the good photovoltaic performance values in this area [8–10]. Benzimidazoles are recently used in optoelectronic technologies for this purpose. Their high electron transporting properties due to electron withdrawing imine (C═N) bond in their structure are important in electrochromic applications [11]. Benzimidazole-based organic dyes, possessing triphenylamine donors and cyanoacrylic acid acceptors with the bithiophene π-bridges combined in different nuclear positions of benzimidazole were studied in dye sensitized solar cells (DSSCs). These benzimidazole derivatives led to remarkable variations in intramolecular charge transfer (ICT) absorption, electron injection efficiency, and charge recombination kinetics giving high power conversing efficiencies [12,13].

They are generally preferred as donor components in OPV devices due to their more appropriate energy levels [14]. Electron mobility of its conjugated structure with perylene imide chromophore is reported as 4×10^{-3} $cm^2/V \cdot s$ [15]. Also, photovoltaic performance and mobility measurement of a perylene diimide-benzimidazole type structure are investigated in the literature [16].

In this study, we have designed three novel benzimidazole-thiophene based small molecules with different electronic moieties, coded as **DTBI(1–3)**, in order to investigate their electronic performances in organic optoelectronic applications. We have preferred two thiophene linkers between the donor benzimidazole and acceptor propan-1-one group aiming to enhance the carrier mobility and charge separation ability of benzimidazole main core in device configuration.

* Corresponding author.
E-mail address: haluk.dincalp@cbu.edu.tr (H. Dinçalp).

http://dx.doi.org/10.1016/j.saa.2017.07.007
1386-1425/

Thiophene π-bridge shows good charge carrier mobility [17] and contributes to the OPV performance of dithienosilole-bithiazole backboned copolymer in the literature [18,19]. DTBIs have been used as additive materials in bulk heterojunction solar cells (BHJ-SCs) in this study. We have fabricated the photovoltaic devices by adding DTBI derivatives with different blending ratios in a configuration of ITO/PEDOT:PSS/P3HT:**DTBI(1–3)**:PCBM/Ca (30 nm):Al (70 nm) (0.5, 1, and 2 wt%). We have analyzed the ground and excited state properties of the additives both in solution and on thin films combining with their electrochemical compatibilities to the BHJ-SCs.

2. Experimental Section

2.1. General Procedures

For the structural analysis of the synthesized compounds, ^{1}H NMR and ^{13}C NMR were measured on a Bruker 400 MHz spectrometer. FT-IR spectra were recorded on a Perkin Elmer-Spectrum BX spectrophotometer preparing KBr pellets. The LC-MS/MS spectral data of the compounds were obtained on an Agilent Technologies 1560 Infinity liquid chromatography system with a 6420 Triple Quadrupole mass spectrometer equipped with an electrospray ionization (ESI) source. Samples were dissolved in Me-CN solution. The electrospray source of the MS was operated both in positive and negative modes. The UV–vis absorption spectra were recorded with a Perkin Elmer Lambda 950 spectrophotometer in solutions and on quartz substrates. Fluorescence quantum yields have been determined using quinine sulfate dehydrate as a reference standard using the equation below:

$$\Phi_F = \Phi_R \frac{I}{I_R} \frac{OD_R}{OD} \left(\frac{n}{n_R}\right)^2$$

where Φ_R indicates the fluorescence quantum yields of reference compound. I and I_R are the integrated emission band areas for DTBI dye and standard, respectively. OD and OD_R are the optical densities for dye and standard, respectively. *n* indicates the solvent refractive index.

FLS 920 Edinburg fluorescence phosphorescence spectrophotometer was used to determine the fluorescence decay kinetics of the dyes in solution. The fluorescence decay times of the molecules were calculated using the Edinburgh Instruments F900 exponential tail fit method [20] after the data were collected by single photon counting system excited by the laser diode at 368.8 nm. The fitted decay curve was settled by the fitting parameters such as $\chi^2 \leq 1.2$ goodness of fit [21].

Electrochemical characterization of the sensitizers were carried through a CH instruments 660B-Electrochemical Workstation with a standard three-electrode electrochemical compartment in 100 mM [TBA][PF6] solution in Me–CN as the supporting electrolyte. Ag/Ag^{+} and Pt wires were performed as reference and counter electrodes, respectively. A polished glassy carbon was used as working electrode in the measurements at the scan rate of 100 mV/s. Oxidation potential of ferrocene–ferrocenium (Fe/Fe^{+}) couple was detected at +0.66 V for the calculation of the onset values of E_{red}. HOMO and LUMO energy levels of **DTBI(1–3)** dyes were calculated by using the formulas [22]:

$$E_{HOMO} = -e\left(E_{ox}^{onset} + 4.8\right); E_{LUMO} = -e\left(E_{red}^{onset} + 4.8\right)$$

$$E_g^{opt} = {}^{1240}/_{\lambda_{abs}^{onset}}; E_{HOMO} = E_{LUMO} - E_g^{opt}$$

DFT and TD-SCF method calculations were performed using the Gaussian 09W [23]. The geometry of the dye were optimized using density functional theory (DFT) with the hybrid B3LYP/6-31G (d) [24] density functional. Oscillator strength (f) calculated by time dependent density functional theory are presented as 0.2355, 0.0239, and 0.6712 for **DTBI1**, **DTBI2** and **DTBI3**, respectively.

2.2. Materials

3-(*N*,*N*-dimethylamino)phenylboronic acid, 3-methoxybenzeneboronic acid, 3-(trifluoromethyl)phenylboronic acid, tetrakis(triphenylphosphine)palladium(0) ($Pd(PPh_3)_4$), 1-(5-bromo-2-thienyl)propan-1-one, 5-formyl-2-thienyl boronic acid, 2,1,3-benzothiadiazole, [6,6]-phenyl C_{61}-butyric acid methyl ester (PCBM), [6,6]-phenyl C_{71}-butyric acid methyl ester ($PC_{71}BM$), and poly(3-hexylthiophene-2,5-diyl) (P3HT) were purchased from Sigma Aldrich Company. Benzene, bromine, hydrogen bromide solution (47%), sodium borohydride, tetrahydrofuran, methanol, ethanol, *n*-hexane, and diethyl ether were purchased from Merck Company. Sodium carbonate (from Carlo Erba) and $CoCl_2 \cdot 6H_2O$ (from Alfa Aesar) were used as received. 4,7-Dibromo-2,1,3-benzothiadiazole, **BT1**, and **BT2** were synthesized according to reference [25]. Scheme 1a and b present the synthesis of **DTBI(1–3)** dyes and their precursors.

2.3. OPV Device Fabrication, Photovoltaic Measurements and Testing

Solar cells were fabricated with the conventional structures given below:

ITO/PEDOT:PSS/**DTBI(1–3)**:$PC_{71}BM$/Ca (30 nm):Al (70 nm) (1:1 *w*/*w*).

ITO/PEDOT:PSS/P3HT:**DTBI(1–3)**:PCBM/Ca (30 nm):Al (70 nm) (0.5, 1, and 2 wt%).

Photovoltaic devices were fabricated on an indium tin oxide (ITO) coated glass substrate (from Delta Tech. Corp., 2.5 × 2.5 cm in size) with R_{sheet}: 10 Ω/sq conductivity. ITO glass substrates were cleaned using the following sequential steps: rinsing with deionized water, sonication in acetone, and isopropanol for 15 min each; and dried with nitrogen. Finally, the substrates were treated with oxygen plasma with 5 cm^3 in volume under the operating pressure of 10^{-2} mbar with 60 W power for 5 min. A filtered dispersion of PEDOT:PSS (AL4083) in water was spin-coated with 4000 rpm for 30 s, followed by annealing at 120 °C for 30 min under ambient conditions. Photoactive components were dissolved at concentrations of 2 wt% from *o*-dichlorobenzene solution in different mass ratios. A mixture of **DTBI(1–3)**:$PC_{71}BM$ (1:1 wt ratio) was spin-coated with 1000 rpm on the top of PEDOT:PSS layer. The active layer of P3HT:PCBM with **DTBI(1–3)** dopants (0.5, 1, and 2 wt%) was formed by spin-coating with 1500 rpm. The films were dried at 120 °C for 30 min. The Ca/Al (30 nm/70 nm) metal electrode was thermally deposited. All organic layers were spin casted with spin-coater flashed with nitrogen and, then devices were completed by the evaporation of the metal electrode in thermal evaporator integrated into MBRAUN 200B glove box.

The current-voltage characteristics of the photovoltaic cells were measured in a glove box using a computer controlled Keithley 2400 digital source meter under illumination of simulated AM1.5G light with the intensity of 100 mW/cm^2. The surface of the thin films was investigated by Ambious Technology Q-Scope 250 Model Atomic Force Microscope in non-contact mode.

2.4. Synthesis

2.4.1. Synthesis of 4,7-Bis[3-(trifluoromethyl)phenyl]-2,1,3-benzothiadiazole (*BT3*)

4,7-Dibromo-2,1,3-benzothiadiazole (77 mg, 0.26 mmol) was dissolved in 35 mL of benzene, then 15 mL 2 M aqueous solution of sodium carbonate solution was added. The mixture was heated to 65 °C for 10 min under an argon atmosphere. 7 mL ethanol solution of 3-(trifluoromethyl)phenyl boronic acid (100 mg, 0.53 mmol) was added dropwise to this solution. $Pd(PPh_3)_4$ catalyst (20 mg, 17 μmol) was added to the mixture, then the solution was stirred at 85 °C for 2 h under an argon atmosphere. After the reaction was completed, the mixture was poured into water and extracted with chloroform (3 × 50 mL). The organic layer was dried over anhydrous magnesium sulfate and

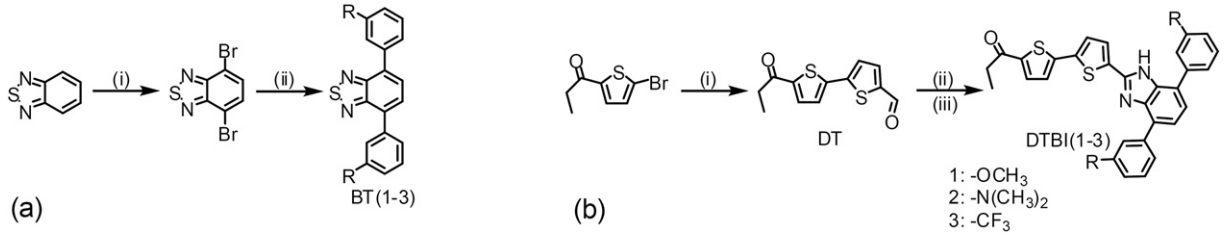

Scheme 1. Synthesis of **DTBI(1–3)** molecules and their precursors **BT(1–3)** benzimidazoles. (a) (i) Br_2/HBr, 120 °C [26]; (ii) boronic acid derivative, 2 M Na_2CO_3, $Pd(PPh_3)_4$, EtOH/benzene, 85 °C [27]. (b) (i) 5-Formyl-2-thienylboronic acid, 2 M Na_2CO_3, $Pd(PPh_3)_4$, THF, 75 °C [27]; (ii) **BT(1–3)**, $NaBH_4$/$CoCl_2 \cdot 6H_2O$, EtOH/THF, 80 °C [28]; (iii) methanol, room temperature (for **DTBI1** and **DTBI3**); $CoCl_2 \cdot 6H_2O$, EtOH/THF, 80 °C (for **DTBI2**) [29].

evaporated in vacuum to dryness. The residue was separated by column chromatography on silica gel using *n*-hexane:ethyl acetate (4:1) as eluent. Yield: 70%, FT-IR (KBr pellet, cm^{-1}): 3066 (aromatic ν_{C-H}), 1610, 1574 (aromatic $\nu_{C=C}$), 1554, 1486, 1432, 1340, 1318, 1270, 1228, 1160, 1122, 1074, 906, 850, 800, 696 cm^{-1}. ^1H NMR (400 MHz, $CDCl_3$ δ 7.27 ppm): δ = 8.26 (2H, s), 8.21 (2H, d, J = 7.6 Hz), 7.87 (2H, s), 7.72 (4H, dt, J_1 = 15.4 J_2 = 7.6 Hz) ppm. ^{13}C NMR [100 MHz, $CDCl_3$ δ 77.3 (3 peaks)]: δ = 154.5, 138.5, 133.2, 132.0, 131.7, 129.7, 128.9, 126.7, 125.8, 123.5 ppm.

*2.4.2. Synthesis of 5′-Propionyl-2,2′-bithiophene-5-carbaldehyde (**DT**)*

To a solution of 1-(5-bromo-2-thienyl)propan-1-one (64 mg, 0.29 mmol) in 12 mL of THF was added 6 mL 2 M aqueous solution of Na_2CO_3. Subsequently, ($Pd(PPh_3)_4$) catalyst (13.3 mg, 11.5 $\times 10^{-3}$ mmol) was added, then the mixture was stirred at 45 °C for half an hour. 5-Formyl-2-thienylboronic acid (90 mg, 0.58 mmol) in 6 mL of THF was added dropwise and the mixture was stirred at 75 °C for 21 h under an argon atmosphere. Then the reaction mixture was poured into water and extracted with chloroform (3 × 50 mL). The organic layer was dried over anhydrous magnesium sulfate and evaporated in vacuum to dryness. The residue was separated by column chromatography on silica gel using *n*-hexane:ethyl acetate (4:1) as eluent. Yield: 83%, FT-IR (KBr pellet, cm^{-1}): 2924 and 2854 (aliphatic ν_{C-H}), 1657 (ketone $\nu_{C=O}$), 1651 (aldehyde $\nu_{C=O}$), 1512 (aromatic $\nu_{C=C}$), 1437, 1287, 1229, 1062, 875, 793, 666 cm^{-1}. ^1H NMR (400 MHz, $CDCl_3$, δ 7.27 ppm): δ = 9.90 (1H, s), 7.71 (1H, d, J = 4.0 Hz), 7.64 (1H, d, J = 4.0 Hz), 7.37 (1H, d, J = 4.0 Hz), 7.34 (1H, d, J = 4.0 Hz), 2.93 (2H, q, J = 7.3 Hz), 1.24 (3H, t, J = 7.3 Hz) ppm. ^{13}C NMR [100 MHz, $CDCl_3$ δ 77.4 (3 peaks)]: δ = 194.5, 183.6, 146.2, 145.3, 144.1, 143.7, 137.8, 133.0, 127.1, 126.6, 32.6, 8.5 ppm.

*2.4.3. Synthesis of 1-{5′-[4,7-Bis(3-methoxyphenyl)-1H-benzimidazol-2-yl]-2,2′-bithien-5-yl}propan-1-one (**DTBI1**)*

A mixture of compound **BT1** (0.1 g, 0.29 mmol), $NaBH_4$ (27 mg, 0.71 mmol), and 10% mol $CoCl_2 \cdot 6H_2O$ (4.8×10^{-2} M, 29 μmol) were dissolved in 4 mL of EtOH:THF (3:1) solvent system. The mixture was stirred under reflux for 4 h under an argon atmosphere. Black solid Co_2B was formed instantly and H_2S evolution was noted in a few minutes. Then the mixture was cooled to room temperature and filtered to separate the black solid. The solvent was evaporated and, then 50 mL of water was added to the crude solid. The organic product was extracted with Et_2O (3 × 30 mL). The combined organic extracts were dried over Na_2CO_3 and the solvent was removed. The resulted bisamine, 3,3″-dimethoxy-1,1′:4′,1″-terphenyl-2′,3′-diamine, was unstable under air and used for the following step immediately. Yield: 93%.

5′-Propionyl-2,2′-bithiophene-5-carbaldehyde (**DT**) (35 mg, 0.14 mmol) was added to a solution of bisamine (50 mg, 0.16 mmol) in 23 mL of methanol and, then the reaction mixture was stirred at room temperature for one week. The mixture was filtered off and the crude product was purified chromatographically on silica gel using methylene chloride:*n*-hexane (3:1) as eluent to yield a yellow solid. Yield: 45%, FT-IR (KBr pellet, cm^{-1}): 2924 and 2851 (aliphatic ν_{C-H}), 1662 (ketone $\nu_{C=O}$), 1599, 1581 (aromatic $\nu_{C=C}$), 1439, 1350, 1322, 1272, 1226, 1042, 783, 689 cm^{-1}. ^1H NMR (400 MHz, $CDCl_3$, δ 7.27 ppm): δ = 9.68 (1H, s), 7.82 (1H, s), 7.68 (1H, s), 7.62 (1H, d, J = 4.0 Hz), 7.53 (1H, d, J = 4.0 Hz), 7.42 (5H, m), 7.29 (1H, d, J = 4.0 Hz), 7.24 (1H, d, J = 4.0 Hz), 7.20 (1H, s), 6.98 (2H, s), 3.92 (6H, s), 2.92 (2H, q, J = 7.3 Hz), 1.24 (3H, t, J = 7.3 Hz) ppm (Fig. S1). ^{13}C NMR [100 MHz, $CDCl_3$ δ 77.4 (3 peaks)]: δ = 194.6, 155.4, 147.1, 144.9, 143.5, 140.7, 139.6, 134.4, 133.1, 131.2, 129.4, 127.6, 126.7, 125.6, 124.1, 123.1, 121.5, 114.6, 113.8, 55.7, 32.4, 8.6 ppm (Fig. S2). LC-MS/MS calculated 550, found $[M + H]^+$ 551 and $[M - H]^-$ 549.

*2.4.4. Synthesis of 1-(5′-{4,7-Bis[3-(dimethylamino)phenyl]-1H-benzimidazol-2-yl}-2,2′-bithien-5-yl)propan-1-one (**DTBI2**)*

A mixture of compound **BT2** (0.1 g, 0.27 mmol), $NaBH_4$ (25 mg, 0.66 mmol), and 10% mol $CoCl_2 \cdot 6H_2O$ (4.8×10^{-2} M, 29 μmol) were dissolved in 4 mL of EtOH:THF (3:1) solvent system. The mixture was stirred under reflux for 2 h under an argon atmosphere. Black solid Co_2B was formed instantly and H_2S evolution was noted in a few minutes. Then the mixture was cooled to room temperature and filtered to separate the black solid. The solvent was evaporated and, then 50 mL of water was added to the crude solid. The organic product was extracted with Et_2O (3 × 30 mL). The combined organic extracts were dried over Na_2CO_3 and the solvent was removed. The resulted bisamine, N3,N3,N3″,N3″-tetramethyl-1,1′:4′,1″-terphenyl-2′,3,3′,3″-tetramine, was unstable under air and used for the following step immediately. Yield: 77%.

5′-Propionyl-2,2′-bithiophene-5-carbaldehyde (**DT**) (65 mg, 0.26 mmol) was added to a solution of bisamine (97 mg, 0.28 mmol) in 3 mL of MeCN. Then $CoCl_2 \cdot 6H_2O$ (5 mg, 21 μmol) was added and the reaction mixture was stirred at room temperature for 2 days. The mixture was filtered off and the resulting crude product was adsorbed on silica gel and purified by column chromatography using *n*-hexane:ethyl acetate (4:1) as the eluent to produce **DTBI2** as a yellow solid. Yield: 47%, FT-IR (NaCl disk, cm^{-1}): 3287, 3085, 2925 and 2853 (aliphatic ν_{C-H}), 1659 (ketone $\nu_{C=O}$), 1599, 1574 (aromatic $\nu_{C=C}$), 1493, 1445, 1359, 1322, 1227, 1058, 1000, 937, 801, 776, 697 cm^{-1}.

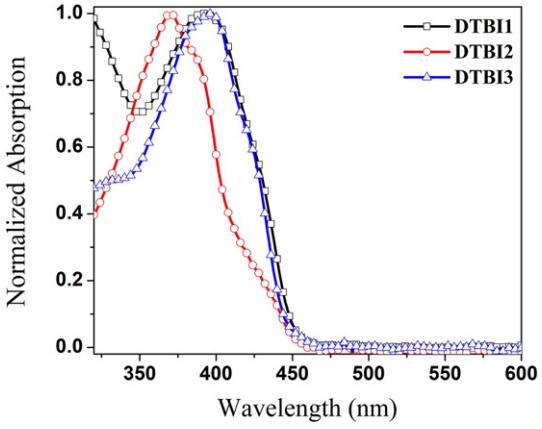

Fig. 1. The normalized UV–vis absorption spectra of **DTBI(1–3)** molecules in toluene solution.

Table 1
Long-wavelength absorption (λ (nm)) and emission (λ_{em} (nm)), fluorescence quantum yields (Φ_F)[a] and fluorescence decay times (τ_f (ns)) of **DTBI(1–3)** molecules in different solvents ($\lambda_{exc} = 365$ nm, $\lambda_{detection} = 550$ nm).

Dyes/solvents	$PhCH_3$				PhCl				EtAc				THF			
	λ_{abs}	λ_{em}	Φ_F	τ_f	λ_{abs}	λ_{em}	Φ_F	τ_f	λ_{abs}	λ_{em}	Φ_F	τ_f	λ_{abs}	λ_{em}	Φ_F	τ_f
DTBI1	396	524	0.87	1.45	396	531	1.00	1.60	396	535	0.78	1.85	396	543	0.74	2.31
DTBI2	374	563	0.21	3.04	376	616	0.08	4.11	367	628	0.02	2.80	367	640	0.03	3.05
DTBI3	396	513	0.88	1.91	396	522	0.77	1.64	396	520	0.75	1.55	396	525	0.82	1.57

[a] Fluorescence quantum yields have been determined using quinine sulfate dihydrate ($\lambda_{exc} = 365$ nm, $\Phi_F = 0.546$, 1 N H_2SO_4) [33].

^{1}H NMR (400 MHz, $CDCl_3$, δ 7.28 ppm): δ = 8.47 (s, 1H), 7.83 (1H, d, J = 8.4 Hz), 7.66 (2H, d, J = 4.0 Hz), 7.47–7.35 (4H, m), 7.30 (1H, d, J = 4.0 Hz), 7.24 (2H, s), 7.18 (1H, d, J = 9.2 Hz), 7.02–6.96 (2H, m), 6.79 (1H, d, J = 9.2 Hz), 3.23 (6H, s), 3.02 (6H, s), 2.94 (2H, q, J = 7.3 Hz), 1.25 (3H, t, J = 7.3 Hz) ppm (Fig. S3). ^{13}C NMR [100 MHz, $CDCl_3$ δ 77.4 (3 peaks)]: δ = 194.2, 183.5, 146.6, 146.1, 145.6, 145.3, 145.0, 144.0, 143.8, 143.4, 139.2, 137.6, 137.5, 133.2, 132.9, 130.7, 127.1, 127.6, 124.0, 32.5, 30.0, 8.5 ppm (Fig. S4). LC-MS/MS calculated 576, found $[M + H]^+$ 577 and $[M - H]^-$ 575.

*2.4.5. Synthesis of 1-(5′-{4,7-bis[3-(trifluoromethyl)phenyl]-1H-benzimidazol-2-yl}-2,2′-bithien-5-yl)propan-1-one (**DTBI3**)*

A mixture of compound **BT3** (80 mg, 0.19 mmol), $NaBH_4$ (30 mg, 0.79 mmol), and 10% mol $CoCl_2 \cdot 6H_2O$ (4.8×10^{-2} M, 29 μmol) were dissolved in 4 mL of EtOH:THF (3:1) solvent system. The mixture was stirred under reflux for 3 h under an argon atmosphere. Black solid Co_2B was formed instantly and H_2S evolution was noted in a few minutes. Then the mixture was cooled to room temperature and filtered to separate the black solid. The solvent was evaporated and, then 50 mL of water was added to the crude solid. The organic product was extracted with Et_2O (3 × 30 mL). The combined organic extracts were dried over Na_2CO_3 and the solvent was removed. The resulted bisamine, 3,3″-bis(trifluoromethyl)-1,1′:4′,1″-terphenyl-2′,3′-diamine, was unstable under air and used for the following step immediately. Yield: 80%.

5′-Propionyl-2,2′-bithiophene-5-carbaldehyde (**DT**) (35 mg, 0.14 mmol) was added to a solution of bisamine (63 mg, 0.16 mmol) in 20 mL of methanol and, then the reaction mixture was stirred at 65 °C for 2 days. The mixture was filtered off and the crude product was purified chromatographically on silica gel using *n*-hexane:ethyl acetate (4:1) as eluent to yield a yellow solid. Yield: 65%, FT-IR (NaCl disk,

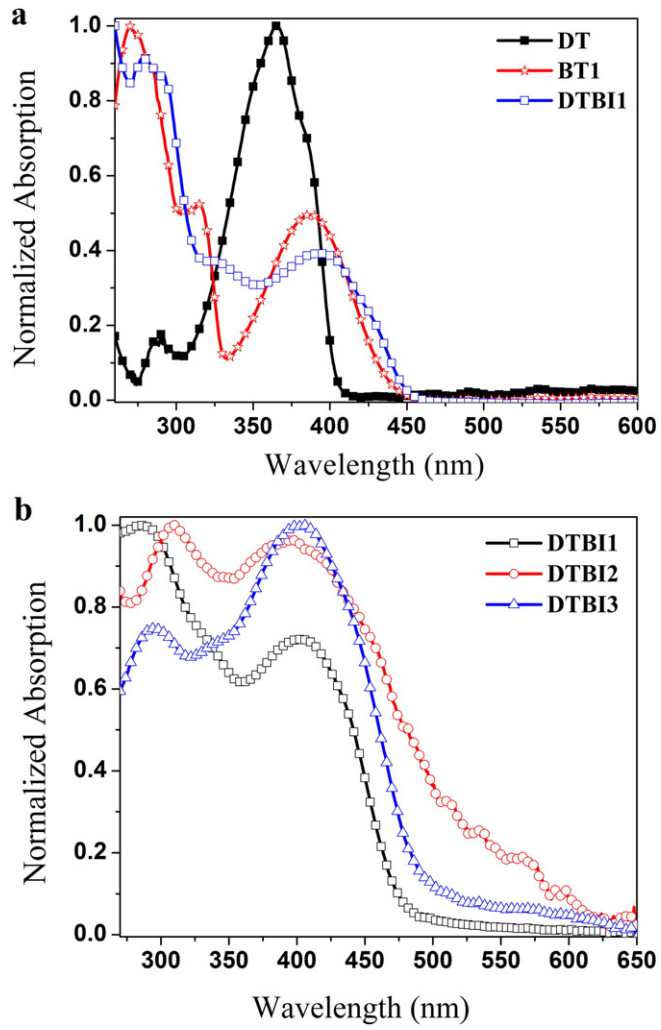

Fig. 2. (a) Comparison of the normalized UV–vis absorption spectra of **DTBI1** molecule with its precursors, **DT** and **BT1** fragment in THF solution. (b) The normalized UV–vis absorption spectra of **DTBI(1–3)** molecules on quartz substrate.

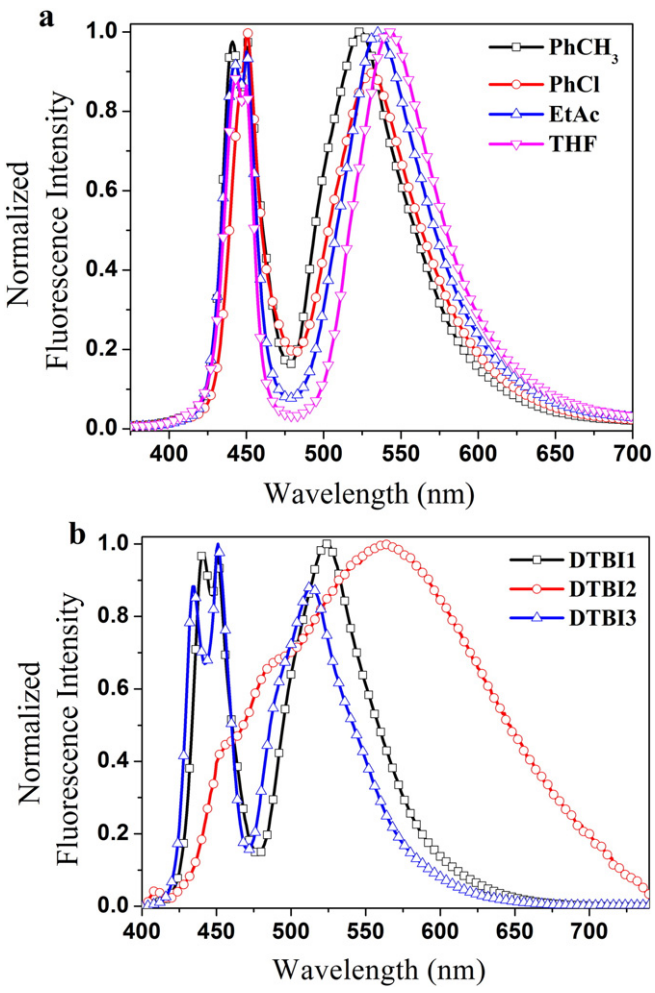

Fig. 3. Comparison of the normalized fluorescence emission spectra of (a) **DTBI1** molecule in different solvents and, (b) **DTBI(1–3)** molecules in toluene ($\lambda_{exc} = 365$ nm).

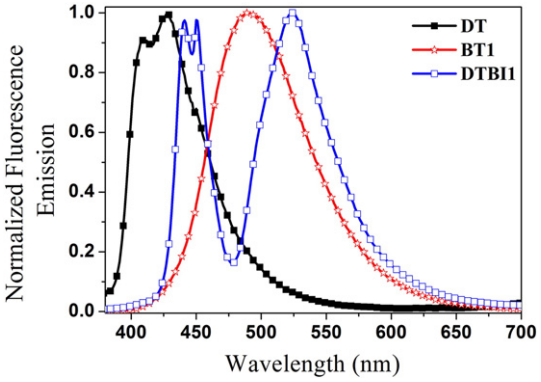

Fig. 4. Comparison of the normalized fluorescence emission spectra of **DTBI1** molecule with its precursors, **DT** and **BT1** fragment in toluene solution (λ_{exc} = 365 nm).

cm^{-1}): 3289, 2979 and 2937 (aliphatic ν_{C-H}), 1650 (ketone $\nu_{C=O}$), 1558, 1532 (aromatic $\nu_{C=C}$), 1482, 1434, 1359, 1336, 1297, 1227, 1166, 1125, 1073, 904, 798, 739, 720, 699 cm^{-1}. ^{1}H NMR (400 MHz, $CDCl_3$, δ 7.27 ppm): δ = 10.27 (1H, s), 8.33 (2H), 7.88 (2H), 7.63–7.56 (8H, m), 7.21 (2H, d, J_1 = 14.8 J_2 = 3.9 Hz), 2.85 (2H, q, J = 7.3 Hz), 1.17 (3H, t, J = 7.3 Hz) ppm (Fig. S5). ^{13}C NMR [100 MHz, $CDCl_3$ δ 77.4 (3 peaks)]: δ = 194.9, 148.0, 144.9, 144.4, 143.4, 139.8, 139.5, 134.1, 133.3, 133.1, 132.3, 129.9, 128.3, 127.1, 126.7, 126.2, 125.6, 124.9, 123.4, 32.5, 8.5 ppm (Fig. S6). LC-MS/MS calculated 626, found $[M + H]^+$ 627 and $[M - H]^-$ 625.

3. Results and Discussion

3.1. Optical Properties and Time Resolved Measurements

Optical properties of **DTBI(1–3)** dyes were studied by taking measurements in different solvents. Fig. 1a shows the normalized UV–vis absorption spectra of **DTBI(1–3)** dyes in toluene, and the corresponding optical data are given in Table 1. The shapes and the band positions of the absorption spectra of both **DTBI1** and **DTBI3** dyes are not affected by the solvent change. They exhibit typical absorption band around 396 nm assigned to the n–π^* transition, which predominantly originates in HOMO-LUMO excitations, and a shallow tail extending out to approximately 450 nm. The absorption spectrum of **DTBI2** dye with donor $N(CH_3)_2$ groups shows blue-shifts by 20–29 nm in the studied solvents. It was noted that the absorption maximum around 374 nm could be attributed to an intramolecular charge transfer (ICT) complex in the ground state between the donor $N(CH_3)_2$ groups and acceptor benzimidazole core. It was reported that greater charge transfer occurs

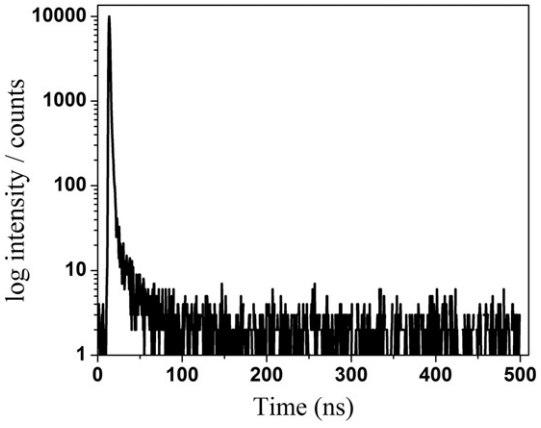

Fig. 5. Fluorescence decay analysis of **DTBI1** molecule in ethyl acetate solution ($\lambda_{detection}$ = 550 nm).

Table 2
Fluorescence decay times ($\tau_{f(n)}$ (ns)), residual values ($\alpha_{(n)}$), radiative rate constants ($k_r \times 10^8$ (s^{-1})) and non-radiative rate constants ($k_{nr} \times 10^8$ (s^{-1})) of **DTBI(1–3)** molecules in different solvents at the collected emission wavelength of 450 nm.

Dyes/solvent		χ^2	$\tau_{f(1)}$	α_1	$\tau_{f(2)}$	α_2	k_r	k_{nr}
DTBI1	$PhCH_3$	1.19	0.79	84.1	2.16	15.9	5.9	0.9
	PhCl	1.14	0.74	53.6	1.82	46.4	7.8	0.0
	EtAc	1.10	0.86	66.5	2.09	33.5	5.3	1.5
	THF	1.20	1.21	76.0	3.83	24.0	2.9	1.0
DTBI2	$PhCH_3$	1.14	2.32	79.3	5.86	20.7	0.5	1.9
	PhCl	1.03	2.33	67.1	6.33	32.9	0.2	2.1
	EtAc	1.16	2.00	74.1	6.73	25.9	0.05	2.3
	THF	1.16	1.93	72.0	6.26	28.0	0.07	2.4
DTBI3	$PhCH_3$	1.00	0.51	48.4	1.82	51.6	7.6	1.0
	PhCl	0.99	0.50	39.8	1.87	60.2	6.5	1.9
	EtAc	1.03	0.43	32.6	1.67	67.4	7.1	2.4
	THF	1.07	0.52	42.2	1.62	57.8	7.7	1.7

Photophysical parameters are calculated with the formulas: $\tau_f = \sum \tau_{f(n)} / n$, $k_r = \Phi/\tau_f$, $k_{nr} = (1 - \Phi)/\tau_f$ [34,35].

from nitrogen atom of $N(CH_3)_2$ group to the phenanthrimidazole type molecule in the literature [30].

Fig. S7(a–c) report the molar extinction coefficients of **DTBI(1–3)** molecules. The higher absorptivity are found (regardless for the solvent) for dyes as **DTBI2** > **DTBI3** > **DTBI1**. **DTBI1** has the lowest molar absorptivity at 396 nm in THF solution (1.09×10^3 M^{-1} cm^{-1}) while this value for **DTBI3** is about 3.2×10^4 M^{-1} cm^{-1}. The lowest absorptivities were observed in toluene solution for all molecules.

To further elucidate the structural correlations, we compared to UV–vis absorption spectra of **DTBI(1–3)** molecules with respect to their fragments, bithienyl group (**DT**) and benzimidazole structures (**BT1–3**) in THF solution. These comparisons are illustrated in Figs. 2a and S8(a–b). Thiophene π-bridge of **DT** fragment and heteroaromatic structure of **BT1** benzimidazole contribute the equally to the absorption of **DTBI1**. Therefore, the amount of delocalization in **DTBI1** structure shifts the absorption peak to a higher value (396 nm) in THF solution compared to 365 nm for **DT** and 387 nm for **BT1**, and a shoulder seems to appear on the lower energy side of the spectrum. In case of **DTBI2**, absorption appears to be dominated by the **DT** fragment while the low energy shoulder nicely overlaps with the **BT2** absorption, as shown in Fig. S8a.

Fig. 2b shows the absorption behavior of **DTBI(1–3)** dyes on quartz substrate. The thin films show a similar absorption trend; however, the films show slightly larger red-shifts as compared to that of the solution. **DTBI1**, **DTBI2**, and **DTBI3** gave broad absorption bands centered at 405, 394, and 404 nm, respectively, and with tails extending up 625 nm region.

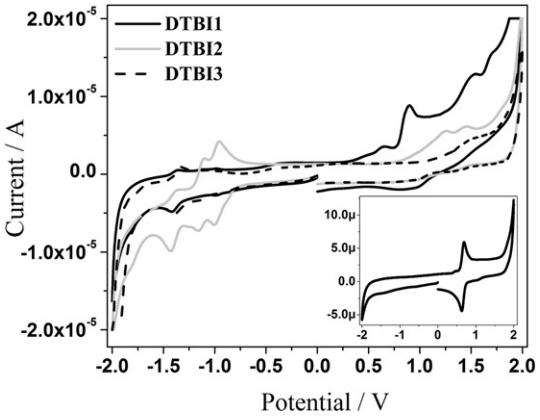

Fig. 6. Cyclic voltammograms of **DTBI(1–3)** molecules on glassy carbon working electrode in 0.1 M [TBA][PF6]/Me-CN (Scan rate: 100 mV/s). Inset shows the cyclic voltammograms of internal reference (ferrocene) under the same conditions.

Table 3
Electrochemical values and HOMO-LUMO energies of **DTBI(1–3)** molecules with respect to the vacuum level.

Dyes	E^0_{red3} (V)	E^0_{red2} (V)	E^0_{red1} (V)	E^0_{ox1} (V)	E^0_{ox2} (V)	E^0_{ox3} (V)	E^0_{ox4} (V)	LUMO (eV)	HOMO (eV)	E_{0-0}[a] (eV) (abs)
DTBI1	–	−1.39	−0.97	0.65	0.90	1.51	1.68	−3.17	−5.88	2.71
DTBI2	−1.40	−1.13	−0.98	1.24	1.45	–	–	−3.16	−5.90	2.74
DTBI3	−1.35	−1.16	−0.92	1.48	–	–	–	−3.22	−5.90	2.68

[a] The zeroth–zeroth transition E_{0-0} values were estimated from the intersection of the apsis and the straight line which is drawn from the red side of the UV–vis absorption band in chlorobenzene solution.

UV–vis absorption spectra of **DTBI(1–3)** molecules calculated by TDDFT measurements were presented in Fig. S9. Similar absorption trends; but blue-shifted wavelength numbers were found for **DTBI1**, **DTBI2**, and **DTBI3** at about 355, 375, and 350 nm, respectively. The excitation energies for low-lying valence excited states of **DTBI1**, **DTBI2**, and **DTBI3** molecules were underestimated by TDDFT approximation as 2.98 eV, 2.51 eV, and 3.18 eV, respectively.

Fig. 3a and b show the normalized fluorescence emission spectra of **DTBI(1–3)** dyes in different solvents. When the dyes are excited at 365 nm, they exhibit two emission bands, one of them is located around 450 nm, and the others are at longer wavelengths. A serious change on emission maxima is observed depending on the electronic nature of the used solvents. **DTBI2** dye gives a remarkable red-shift from 563 nm in toluene to 640 nm in THF solution. It is noted that such a kind of solvatochromic shift can be related to the formation of ICT states of **DTBI2** dye also accounting for the larger Stokes shift.

Fig. 4 gives a comparison of the normalized fluorescence emission spectra of **DTBI1** with its precursors, **DT** and **BT1** fragment in toluene solution at the excitation wavelength of 365 nm. The emission peaks of **DT** were located at 408 nm (0–0) and 427 nm (0–1). **BT1** gives one broad emission band centered at 491 nm. Interestingly, luminescence emission seems to arise from **DT** fragment at 440 nm and 450 nm, and from **BT1** fragment in **DTBI1**. Each emission peak indicates its belonging fragment. Also, the absorption spectrum of acceptor **DT** could not overlap with the fluorescence emission spectrum of benzimidazole donor side, as a result no resonance energy transfer occurs in the structures of **DTBI1** and **DTBI3** dyes. **DTBI2** dye gives one broad emission spectrum centered at 640 nm as shown in Fig. S10a, **DTBI3** structure illustrates

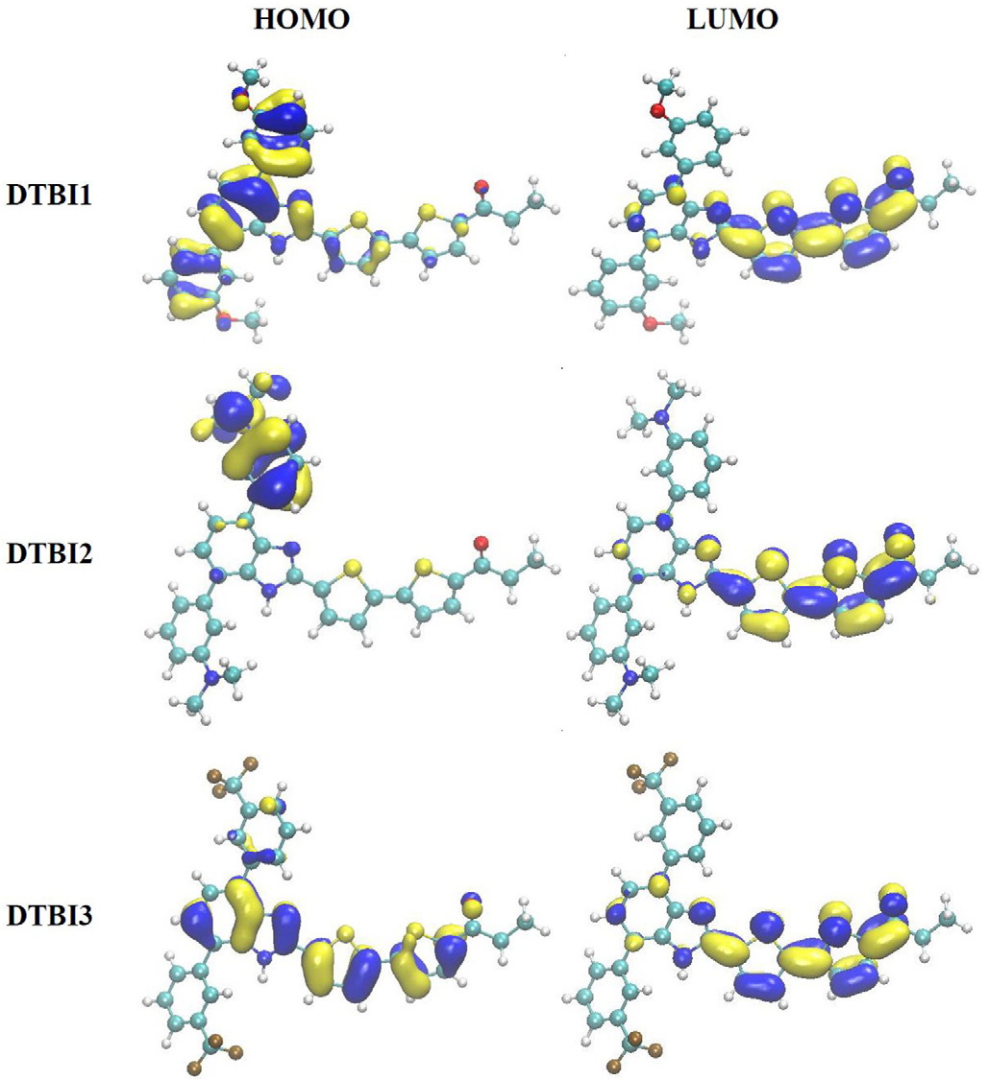

Fig. 7. HOMO and LUMO distributions of the geometry-optimized structures of **DTBI(1–3)** molecules.

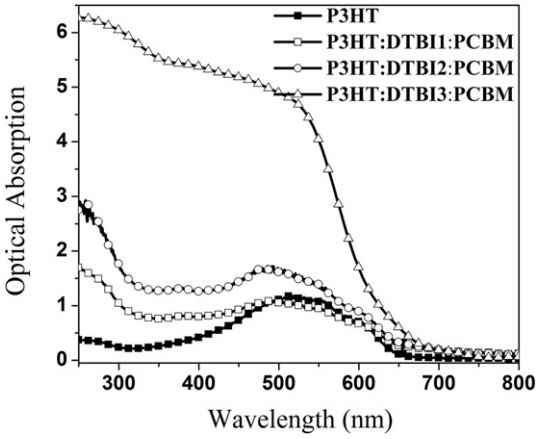

Fig. 8. Comparison of the UV–vis absorption spectra of the P3HT:**DTBI(1–3)**:PCBM (0.99:0.01:1) blends coated on quartz substrate.

double band of fluorescence as shown in Fig. S10b. It was worth noting that this type of dual luminescence is generated from the studied dyes owing to the presence of two excited forms, **DT** moiety and BT core alone, with their different photophysical properties in apolar toluene and other slightly less polar solvents. This dual luminescence is associated with the lack of effective conjugation between the molecule fragments so that each domain behaves like independent parts. As the energy gap between **DT** moiety and BT core depends on large Stokes shift, the energy gap can be tuned to get dual emission. Dual luminescence may arise from any two different states with emission in the violet and green of the visible spectrum.

Fig. 5 and Table 1 summarizes the fit decay results obtained from the single photon counting experiments. The fluorescence decay times of the molecules can be analyzed as mono-exponential decays with short decay times around 1.45–2.31 ns for **DTBI1** dye, 2.80–4.11 ns for **DTBI2** dye, and 1.55–1.91 ns for **DTBI3** dye depending on the used solvents. These time decays are typical on the pristine benzimidazole core [31,32]. Note that the much longer decay times for **DTBI2** dye are evaluated in terms of the decay reaction from the ICT state to the ground state.

The fluorescence quantum yields (Φ_F) of **DTBI(1–3)** dyes were calculated with reference to quinine sulfate dihydrate in four different solvents. While Φ_F values of **DTBI1** and **DTBI3** dyes are reported as between 0.74 and 1.0, Φ_F values are fairly low for **DTBI2** dye in the studied solvents ($\Phi_F \leq 0.08$, except toluene). These much lower values together with the longer lifetime as compared to the **DTBI1** and **DTBI3** dyes can be ascribed to the poor orbital overlap between the LUMO and HOMO energy levels of the molecules. This leads to the emission quenching. In toluene solution, possibly, solvent molecules do not strongly interact with the dye. For this reason, a small part of the emission is quenched and Φ_F values of **DTBI2** in toluene reaches to its maximum value of 0.21.

Also, we have collected the emission data using single photon timing measurements at 450 nm, mainly indicating the **DT** fragment emission, and all decay times are summarized in Table 2. The measurements were analyzed with bi-exponential decay model with short-lived component (much higher amplitude ratio) indicating the decay profile of **DT** fragment. Other long-lived component with much lower amplitude ratio belongs to the benzimidazole fragment. The radiative rate constants of **DTBI2** in the studied solvents are much quite lower (0.05–0.50 $\times 10^8$ s^{-1}) as compared to other dyes when two $N(CH_3)_2$ groups are

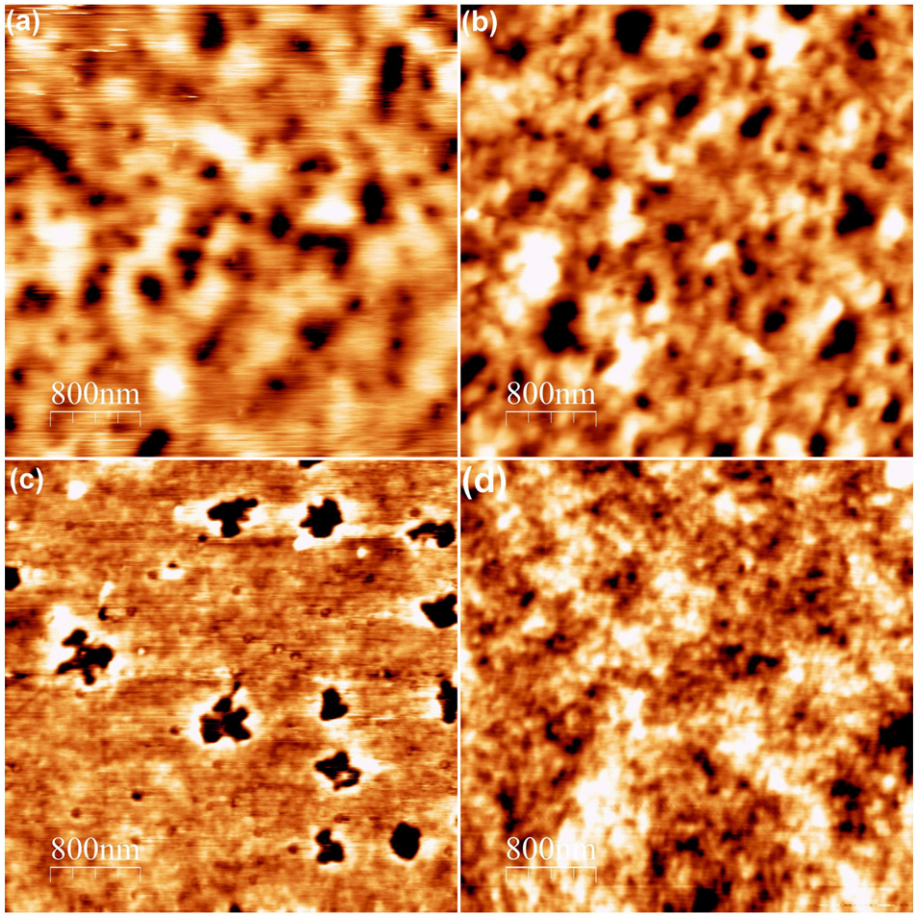

Fig. 9. AFM images (4 μm × 4 μm) of (a) **DTBI1**, (b) **DTBI2**, (c) **DTBI3** and (d) P3HT:**DTBI2**:PCBM (0.995:0.005:1) blend films spin-coated from chloroform solution.

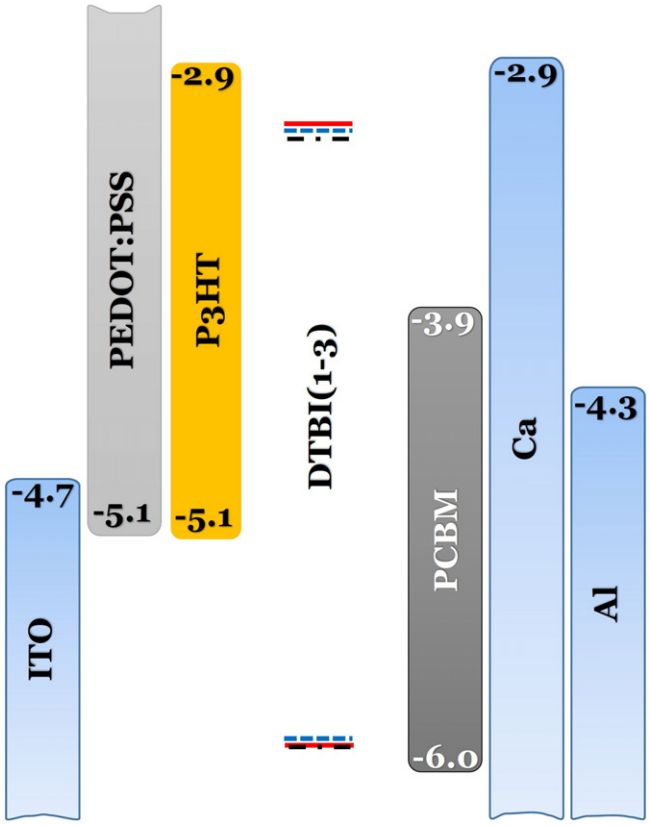

Fig. 10. Energy levels of components for ITO/PEDOT:PSS/P3HT:**DTBI(1–3)**:PCBM/Ca (30 nm):Al (70 nm) photovoltaic device (…: **DTBI1**, —: **DTBI2,** and -·-: **DTBI3**; HOMO and LUMO energy levels are extracted from Table 3).

attached to benzimidazole core. The radiative rate constants get the highest values for **DTBI3** dye ($k_r = 6.5–7.7 \times 10^8\ s^{-1}$) in all solvents when compared to that of other studied dyes.

3.2. CV Measurements and Theoretical Calculations

The HOMO and LUMO energy levels of **DTBI(1–3)** dyes were determined from the electrochemical measurements with cyclic voltammetry. All oxidation and reduction waves are illustrated in Fig. 6, and electrochemical data are summarized in Table 3. More positive potentials indicate the mono- or bis-thiophene ring oxidation. At lower potentials, oxidations are attributed to the formation of aryl benzimidazole species. These peaks are strongly dependent on the substitution of benzimidazole with —OCH_3 or —$N(CH_3)_2$ groups and their electron donating abilities. Also, **DTBI3** exhibits only one oxidation wave at 1.48 V, indicating the formation only thiophene cation. The peaks of the benzimidazole oxidation in **DTBI3** could not easily seen because of the strong electron withdrawing property of —CF_3 groups. The first reduction potentials of **DTBI1**, **DTBI2**, and **DTBI3** dyes are at about −0.97, −0.98, and −0.92 V, which correspond to LUMO energy levels of −3.17, −3.16, and −3.22 eV, respectively. The much easier

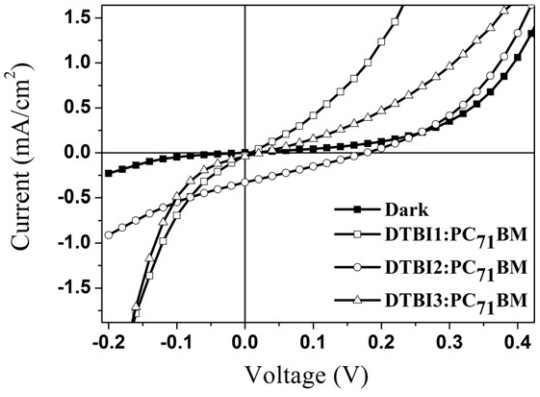

Fig. 11. J–V curves of photovoltaic devices using **DTBI(1–3)**:$PC_{71}BM$ blends as active layers.

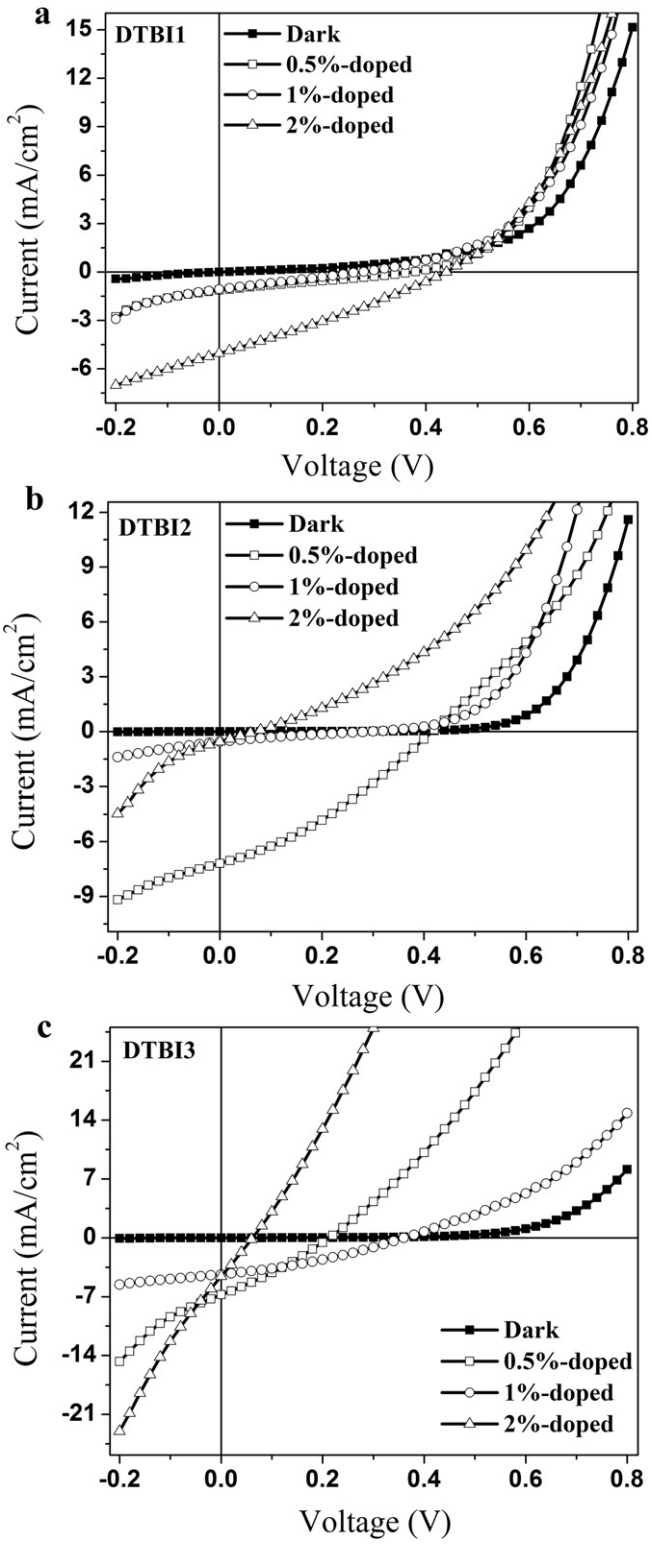

Fig. 12. J–V curves of photovoltaic devices using P3HT:**DTBI(1–3)**:$PC_{71}BM$ blends as active layers with different dopant ratios for (a) **DTBI1**, (b) **DTBI2** and (c) **DTBI3** additives.

reduction of **DTBI3** at −0.92 V is attributed to the presence of —CF_3 groups having more electron withdrawing capacity as compared to the other substituents. Therefore, the incorporation of —CF_3 groups have a considerable effect on their LUMO and band gap values.

Fig. 7 displays the plots of the frontier orbitals. For **DTBI1** dye, the HOMO is delocalized over benzimidazole core and extending over the phenyl rings while the LUMO is extended along the thiophene rings. For **DTBI2** dye, the HOMO is mainly localized on one of the phenyl ring linked to the *N*,*N*-dimethylamino group while the LUMO is mainly contributed by the thiophene rings. HOMO to LUMO excitation for both **DTBI1** and **DTBI2** dyes may result in charge transfer from the benzimidazole side to the thiophene side. Both the HOMO and LUMO for **DTBI3** dye are well delocalized onto thiophene and benzimidazole rings. However, there is a little contribution to the LUMO by the benzimidazole group, indicating the electron flowing to the thiophene rings in the excited states.

3.3. Evaluation of the Dyes in Photovoltaic Applications

In order to get insight into potential usage of the synthesized **DTBI(1–3)** dyes in conventional binary and ternary BHJ-SCs as electron or hole transporting materials we have used spin-coated PCBM/$PC_{71}BM$ as acceptor layer and P3HT as donor layer. Fig. 8 displays the UV–vis absorption spectra of thin films for **DTBI(1–3)** dyes with 1 wt% dopant ratios into the P3HT:PCBM blend. In general, addition of the dyes increase the maximum absorptivity of P3HT observed around 500–520 nm. In the presence of **DTBI2**, molar absorptivity of P3HT:PCBM at 500 nm is improved from 1 to 2 by the contribution of the light absorbed by **DTBI2** additive as compared to that of **DTBI1** additive. When **DTBI1** is replaced by **DTBI3** additive, there is a more pronounced increase in absorptivity from 1 to 5. This significant rise in absorption behavior of the blend may be attributed to the good quality of **DTBI3** covering and homogeneity of the films. We recorded AFM images of **DTBI(1–3)** thin films spin-coated from chloroform solution, as shown in Fig. 9(a–c). The average root-mean-square roughnesses (R_{rms}) of the films of pristine **DTBI1**, **DTBI2**, and **DTBI3** structures are 1.42, 6.33, and 0.57, respectively. It is noted that there is a good connection between the fluorine groups of the —CF_3 substituents of **DTBI3** and the Si groups attached to the surface of the glass. Fig. 9d displays the AFM image of P3HT:**DTBI2**:PCBM thin film doped with 0.5 wt% of the dye to investigate the quality of the blend, which is important point in the interpenetration of networks between the donor and acceptor units. R_{rms} value for this blend is reported as 0.83. This value indicates that **DTBI2** film possessed finely mixed morphology.

Fig. 10 summarizes the HOMO-LUMO energy levels of P3HT, PCBM, and **DTBI(1–3)** dyes as determined by electrochemistry. The LUMO levels of **DTBI(1–3)** are located between the LUMOs of P3HT and PCBM, enabling the electron transfer between them. This energy alignment is true for HOMO levels, allowing the hole transfer process. This kind of energy design for the synthesized dyes is suitable for contribution to charge transfer in such kind of ternary system.

Photocurrent–voltage (J–V) curves of the fabricated BHJ-SCs were recorded under a solar simulator after thermal annealing and, then illustrated in Fig. 11 for binary and Fig. 12(a–c) for ternary blend system. Table 4 summarizes the various photovoltaic parameters such as short circuit current (J_{sc}), open circuit voltage (V_{oc}), fill factor (FF), voltage and current at the maximum power point (V_{mpp} and J_{mpp}), and power conversion efficiency (PCE) of the devices compared to the reference cell of P3HT:PCBM (PCE:2.51). While **DTBI1** does not give any photovoltaic response in the device using **DTBI1**:$PC_{71}BM$ as active layer at the donor/acceptor (1:1 *w*/*w*) weight ratio, **DTBI2** and **DTBI3** donors in the similar configuration give PCE values of 0.01 and 0.0001, respectively. Active layer of **DTBI2** with $PC_{71}BM$ provides a greater J_{sc} value of 0.32 mA/cm^2 with V_{oc} and FF of 180 mV and 0.25, respectively, than that of the device incorporating **DTBI3** blended with $PC_{71}BM$ (J_{sc}: 0.03 mA/cm^2 V_{oc}: 20 mV FF: 0.16).

The device with 0.5 wt% doping ratio of **DTBI1** into the P3HT:PCBM provided a J_{sc} of 1.14 mA/cm^2, a V_{oc} of 380 mV, and FF of 0.25, resulting the PCE value of 0.11. In contrast, the devices based on **DTBI2** and **DTBI3** dyes with the same doping ratio showed a markedly improved performance with PCE values of 0.98 and 0.42, respectively. This relatively poor efficiency for **DTBI1** is probably explained by the depressed charge transportation which is caused by the methoxy substituents of the structure in this blend. More interestingly, better PCE was achieved from P3HT:**DTBI1**:PCBM solar cell at 2 wt% doping weight ratio than that of at 0.5 wt%. The device based on **DTBI1** additive at 2 wt% gave a slightly enhanced performance with a J_{sc} of 5.03 mA/cm^2, a V_{oc} of 440 mV, and FF of 0.28, yielding the PCE value of 0.63. This much better J_{sc} performance may be related to good carrier mobility and morphology as compared to the presence of **DTBI2** and **DTBI3** additives.

At a dye doping ratio of 1 wt%, P3HT:**DTBI3**:PCBM solar cell showed the best PCE of 0.65 with a J_{sc} of 4.10 mA/cm^2, a V_{oc} of 500 mV, and FF of 0.31. This PCE value is more related its absorption behavior in the blend. **DTBI3** is the strongest absorption with 5 times higher molar absorptivity at wavelength of 520 nm, **DTBI3** has 5 times higher molar absorptivity than that of **DTBI1** in P3HT:dye:PCBM blends (see Fig. 8), which plausibly more excitons and charge generation in P3HT:**DTBI3**:PCBM devices than in the other devices.

Table 4
Photovoltaic parameters of normal BHJC devices prepared from **DTBI(1–3)** dyes.

Active layer		V_{oc} (mV)	J_{sc} (mA/cm^2)	FF	V_{mpp} (mV)	J_{mpp} (mA/cm^2)	η
Binary structure	w:w						
P3HT:PCBM	1:1	340	14.65	0.50	220	11.43	2.51
DTBI1:$PC_{71}BM$	1:1	–	–	–	–	–	–
DTBI2:$PC_{71}BM$	1:1	180	0.32	0.25	100	0.15	0.01
DTBI3:$PC_{71}BM$	1:1	20	0.03	0.16	20	0.006	0.0001
Active layer		V_{oc} (mV)	J_{sc} (mA/cm^2)	FF	V_{mpp} (mV)	J_{mpp} (mA/cm^2)	η
Ternary structure	w:w:w						
P3HT:DTBI1:PCBM	0.995:0.005:1	380	1.14	0.25	220	0.50	0.11
P3HT:DTBI1:PCBM	0.99:0.01:1	340	0.96	0.25	180	0.46	0.08
P3HT:DTBI1:PCBM	0.98:0.02:1	440	5.03	0.28	340	2.62	0.63
P3HT:DTBI2:PCBM	0.995:0.005:1	420	7.19	0.32	220	4.46	0.98
P3HT:DTBI2:PCBM	0.99:0.01:1	300	0.56	0.19	140	0.23	0.03
P3HT:DTBI2:PCBM	0.98:0.02:1	100	0.43	0.25	60	0.18	0.01
P3HT:DTBI3:PCBM	0.995:0.005:1	220	6.76	0.28	120	3.52	0.42
P3HT:DTBI3:PCBM	0.99:0.01:1	500	4.10	0.31	260	2.52	0.65
P3HT:DTBI3:PCBM	0.98:0.02:1	60	4.57	0.24	40	1.70	0.06

4. Conclusion

We have designed and synthesized three novel D-A type small molecules, combining benzimidazole-thiophene conjugates arrayed with varied electronic substituents, such as —OCH_3, —$N(CH_3)_2$, —CF_3. The absorption maximum for **DTBI2** dye is blue-shifted likely due to the poor electronic coupling between HOMO and LUMO in this molecule. Remarkable red-shifts and large Stokes shifts for **DTBI2** emissions may point to a stronger excited state distortion (in agreement with the low quantum efficiency of luminescence). Another striking result is the observation of dual luminescence for **DTBI1** and **DTBI3** dyes in the studied solvents. This reaction occurs between structurally and energetically different segments of the whole molecule and therefore results in dual emission, so that the two emission bands are observed and are strongly separated on a wavelength scale. Band gaps increase from 2.68 eV for **DTBI3** to 2.74 for **DTBI2**, with the up-shift of LUMO levels from −3.22 to −3.16 eV, respectively. Photovoltaic properties of the synthesized dyes have been evaluated on both binary and ternary BHJ-SC devices. Substitutions on side chain of benzimidazole core shows considerable effects on optimal photovoltaic performances in terms of values of V_{oc}, J_{sc}, FF, and PCE of the devices, resulted from the substituent structure, optical absorption and morphological change in the film, which can enhance the carrier mobilities.

Supplementary data to this article can be found online at http://dx.doi.org/10.1016/j.saa.2017.07.007.

Acknowledgement

This work was supported by the Scientific and Technological Research Council of Turkey (TUBITAK) with the project number of 113Z250. The authors also thank to Ege University for the support of the use of Gaussian 09W programme for theoretical DFT calculations.

References

[1] L. Vaiana, D. Esteban-Gomez, M. Mato-Iglesias, C. Platas-Iglesias, A. de Blas, T. Rodriguez-Blas, Anion coordination effect on the nuclearity of Co-II, Ni-II, Cu-II, and Zn-II complexes with a benzimidazole pendant-armed crown, Eur. J. Inorg. Chem. 3 (2009) 400–411.
[2] J. Jayabharathi, V. Thanikachalam, K. Jayamoorthy, R. Sathishkumar, Selective quenching of benzimidazole derivatives by Cu^{2+} metal ion, Spectrochim. Acta A 97 (2012) 384–387.
[3] K. Mahiya, P. Mathur, Synthesis of a new N-substituted bis-benzimidazolyl diamide ligand and its trinuclear copper(II) complex: structural and fluorescence studies, Spectrochim. Acta A 113 (2013) 386–392.
[4] D.Y. Lee, N. Singh, D.O. Jang, A benzimidazole-based single molecular multianalyte fluorescent probe for the simultaneous analysis of Cu^{2+} and Fe^{3+}, Tetrahedron Lett. 51 (2010) 1103–1106.
[5] O. Çimen, H. Dinçalp, C. Varlıklı, Studies on UV–vis and fluorescence changements in Co^{2+} and Cu^{2+} recognition by a new benzimidazole–benzothiadiazole derivative, Sensors Actuators B Chem. 209 (2015) 853–863.
[6] J.D. Harris, J. Liu, K.R. Carter, Synthesis of π-bridged dually-dopable conjugated polymers from benzimidazole and fluorene: separating sterics from electronics, Macromolecules 48 (2015) 6970–6977.
[7] J. Ku, S. Song, S.H. Park, K. Lee, H. Suh, Y. Lansac, Y.H. Jang, Palladium-assisted reaction of 2,2-dialkylbenzimidazole and its implication on organic solar cell performances, J. Phys. Chem. C 119 (2015) 14063–14075.
[8] C.J. Brabec, N.S. Sariciftci, J.C. Hummelen, Plastic solar cells, Adv. Funct. Mater. 11 (2001) 15–26.
[9] Y. Lin, Y. Li, X. Zhan, Small molecule semiconductors for high-efficiency organic photovoltaics, Chem. Soc. Rev. 41 (2012) 4245–4272.
[10] G. Yu, J. Gao, J.C. Hummelen, F. Wudl, A.J. Heeger, Polymer photovoltaic cells-enhanced efficiencies via a network of internal donor-acceptor heterojunctions, Science 270 (1995) 1789–1791.
[11] H. Akpınar, A. Balan, D. Baran, E.K. Ünver, L. Toppare, Donor–acceptor–donor type conjugated polymers for electrochromic applications: benzimidazole as the acceptor unit, Polymer 51 (2010) 6123–6131.
[12] G.B. Bodedla, K.R. Justin Thomas, M.-S. Fan, K.-C. Ho, Benzimidazole-branched isomeric dyes: effect of molecular constitution on photophysical, electrochemical, and photovoltaic properties, J. Organomet. Chem. 81 (2016) 640–653.
[13] B. Xu, Y. Li, P. Song, F. Ma, M. Sun, Photoactive layer based on T-shaped benzimidazole dyes used for solar cell: from photoelectric properties to molecular design, Sci Rep 7 (2017) 1–17 45688.
[14] S. Song, H. Han, Y. Kim, B.H. Lee, S.H. Park, Y. Jin, I. Kim, K. Lee, H. Suh, Dimethyl-2H-benzimidazole based small molecules as donor materials for organic photovoltaics, Sol. Energy Mater. Sol. Cells 95 (2011) 1838–1845.
[15] B.R. Sim, B.-G. Kim, J.K. Lee, J.Y. Do, Photovoltaic properties of benzimidazole-derived perylene imides as an n-type material, Thin Solid Films 519 (2011) 8091–8094.
[16] H. Dincalp, O. Cimen, T. Ameri, C.J. Brabec, S. Icli, Synthesis, characterization and optoelectronic properties of a new perylene diimide-benzimidazole type solar light harvesting dye, Spectrochim. Acta A 128 (2014) 197–206.
[17] K. Navamani, G. Saranya, P. Kolandaivel, K. Senthilkumar, Effect of structural fluctuations on charge carrier mobility in thiophene, thiazole and thiazolothiazole based oligomers, Phys. Chem. Chem. Phys. 15 (2013) 17947–17961.
[18] Y. Ie, Y. Aso, Development of donor–acceptor copolymers based on dioxocycloalkene-annelated thiophenes as acceptor units for organic photovoltaic materials, Polym. J. 49 (2016) 13–22.
[19] H. Zheng, C. Gu, Q. Zhu, X. Bao, S. Wen, M. Qiu, D. Zhu, M. Sun, R. Yang, Thiophene π-bridge effect on photovoltaic performances of dithienosilole and bithiazole backboned polymers, J. Appl. Polym. Sci. 132 (2015) 1–8 42798.
[20] J.R. Knutson, J.M. Beechem, L. Brand, Simultaneous analysis of multiple fluorescence decay curves - a global approach, Chem. Phys. Lett. 102 (1983) 501–507.
[21] M. Zuker, A.G. Szabo, L. Bramall, D.T. Krajcarski, B. Selinger, Delta-function convolution method (DFCM) for fluorescence decay experiments, Rev. Sci. Instrum. 56 (1985) 14–22.
[22] J. Pommerehne, H. Vestweber, W. Guss, R.F. Mahrt, H. Bassler, M. Porsch, J. Daub, Efficient 2-layer LEDs on a polymer blend basis, Adv. Mater. 7 (1995) 551–554.
[23] M.J. Frisch, G.W. Trucks, H.B. Schlegel, G.E. Scuseria, M.A. Robb, J.R. Cheeseman, G. Scalmani, V. Barone, B. Mennucci, G.A. Petersson, H. Nakatsuji, M. Caricato, X. Li, H.P. Hratchian, A.F. Izmaylov, J. Bloino, G. Zheng, J.L. Sonnenberg, M. Hada, M. Ehara, K. Toyota, R. Fukuda, J. Hasegawa, M. Ishida, T. Nakajima, Y. Honda, O. Kitao, H. Nakai, T. Vreven, J.A. Montgomery Jr., J.E. Peralta, F. Ogliaro, M.J. Bearpark, J. Heyd, E.N. Brothers, K.N. Kudin, V.N. Staroverov, R. Kobayashi, J. Normand, K. Raghavachari, A.P. Rendell, J.C. Burant, S.S. Iyengar, J. Tomasi, M. Cossi, N. Rega, N.J. Millam, M. Klene, J.E. Knox, J.B. Cross, V. Bakken, C. Adamo, J. Jaramillo, R. Gomperts, R.E. Stratmann, O. Yazyev, A.J. Austin, R. Cammi, C. Pomelli, J.W. Ochterski, R.L. Martin, K. Morokuma, V.G. Zakrzewski, G.A. Voth, P. Salvador, J.J. Dannenberg, S. Dapprich, A.D. Daniels, Ö. Farkas, J.B. Foresman, J.V. Ortiz, J. Cioslowski, D.J. Fox, Gaussian 09, Gaussian, Inc., Wallingford, CT, USA, 2009.
[24] W. Kohn, L.J. Sham, Self-consistent equations including exchange and correlation effects, Phys. Rev. 140 (1965) A1133–A1138.
[25] H. Dinçalp, G. Murat, S. İçli, Improvement of intramolecular charge transfer within a donor–acceptor blend by doping novel synthesized benzothiadiazole small molecules in solid state, Opt. Mater. 36 (2014) 1525–1533.
[26] B.A.D. Neto, A.S.A. Lopes, G. Ebeling, R.S. Goncalves, V.E.U. Costa, F.H. Quina, J. Dupont, Photophysical and electrochemical properties of pi-extended molecular 2,1,3-benzothiadiazoles, Tetrahedron 61 (2005) 10975–10982.
[27] S. Kotha, K. Lahiri, D. Kashinath, Recent applications of the Suzuki-Miyaura cross-coupling reaction in organic synthesis, Tetrahedron 58 (2002) 9633–9695.
[28] B.A.D. Neto, A.S. Lopes, M. Wust, V.E.U. Costa, G. Ebeling, J. Dupont, Reductive sulfur extrusion reaction of 2,1,3-benzothiadiazole compounds: a new methodology using $NaBH_4/CoCl_2 \cdot 6H_2O_{(cat)}$ as the reducing system, Tetrahedron Lett. 46 (2005) 6843–6846.
[29] A.T. Khan, T. Parvin, L.H. Choudhury, A simple and convenient one-pot synthesis of benzimidazole derivatives using Cobalt(II) chloride hexahydrate as catalyst, Synth. Commun. 39 (2009) 2339–2346.
[30] V. Thanikachalam, A. Arunpandiyan, J. Jayabharathi, P. Ramanathan, Photophysical properties of the intramolecular excited charge-transfer states of π-expanded styryl phenanthrimidazoles–effect of solvent polarity, RSC Adv. 4 (2014) 6790–6806.
[31] J. Pina, J.S. Seixas de Melo, R.M. Batista, S.P. Costa, M.M. Raposo, Triphenylamine-benzimidazole derivatives: synthesis, excited-state characterization, and DFT studies, J. Organomet. Chem. 78 (2013) 11389–11395.
[32] T. Inouchi, T. Nakashima, T. Kawai, The origin of the emission properties of π-conjugated molecules that have an acid-responsive benzimidazole unit, Asian J. Org. Chem. 2 (2013) 230–238.
[33] A.M. Brouwer, Standards for photoluminescence quantum yield measurements in solution (IUPAC technical report), Pure Appl. Chem. 83 (2011) 2213–2228.
[34] V. Ramamurthy, K.S. Schanze, Organic Photochemistry and Photophysics, CRC Press, 2005.
[35] P. Suppan, Chemistry and Light, The Royal Society of Chemistry, 1994.